# TRANSIENT BEHAVIOUR OF TROPOSPHERIC OZONE PRECURSORS IN A GLOBAL 3-D CTM AND THEIR INDIRECT GREENHOUSE EFFECTS

R. G. DERWENT[1], W. J. COLLINS[1], C. E. JOHNSON[2] and D. S. STEVENSON[3]

[1]*Climate Research Division, Meteorological Office, Bracknell, U.K.*
[2]*Hadley Centre for Climate Prediction and Research, Meteorological Office, Bracknell, U.K.*
[3]*Department of Meteorology, University of Edinburgh, Scotland*

**Abstract.** The global three-dimensional Lagrangian chemistry-transport model STOCHEM has been used to follow the changes in the tropospheric distributions of the two major radiatively-active trace gases, methane and tropospheric ozone, following the emission of pulses of the short-lived tropospheric ozone precursor species, methane, carbon monoxide, $NO_x$ and hydrogen. The radiative impacts of $NO_x$ emissions were dependent on the location chosen for the emission pulse, whether at the surface or in the upper troposphere or whether in the northern or southern hemispheres. Global warming potentials were derived for each of the short-lived tropospheric ozone precursor species by integrating the methane and tropospheric ozone responses over a 100-year time horizon. Indirect radiative forcing due to methane and tropospheric ozone changes appear to be significant for all of the tropospheric ozone precursor species studied. Whereas the radiative forcing from methane changes is likely to be dominated by methane emissions, that from tropospheric ozone changes is controlled by all the tropospheric ozone precursor gases, particularly $NO_x$ emissions. The indirect radiative forcing impacts of tropospheric ozone changes may be large enough such that ozone precursors should be considered in the basket of trace gases through which policy-makers aim to combat global climate change.

## 1. Introduction

It is well recognised that the emissions of a number of short-lived tropospheric ozone precursor species exert a profound influence on the urban, regional and global distributions of ozone in the troposphere (Leighton, 1961; Crutzen, 1974). These tropospheric ozone precursor species include nitrogen oxides ($NO_x$), methane ($CH_4$), organic compounds, hydrogen and carbon monoxide (CO). Each of these trace gases has important emission sources from human activities and from natural biospheric processes (Olivier et al., 1996). Since tropospheric ozone is an important radiatively active trace gas (Ramanathan et al., 1987), it follows that an indirect greenhouse effect may be, in principle, associated with the emissions of each of these ozone precursor species because of their potential impact on the tropospheric ozone distribution (Derwent, 1990).

In addition to controlling tropospheric ozone production and destruction, the ozone precursor species also control the tropospheric distribution of hydroxyl radicals (Levy, 1971) and hence the oxidising capacity of the troposphere. The

*Climatic Change* **49:** 463–487, 2001.

tropospheric distribution of hydroxyl radicals in turn controls the lifetime and hence global scale build-up of methane (Ehhalt, 1974), another important radiatively active trace gas (Ramanathan et al., 1987). There is therefore the potential for the emissions of the ozone precursor gases to alter the tropospheric distribution of hydroxyl radicals and perturb the global scale build-up of methane (Isaksen and Hov, 1987). It follows then, in principle, that such a perturbation would be associated with an indirect greenhouse effect because of its influence on the global methane distribution.

It has been difficult in the past to assess the magnitudes of these indirect ozone and methane greenhouse effects associated with the emissions of the tropospheric ozone precursors. Initial estimates varied widely in both sign and magnitude and failed to take into account all of the important impacts on the global distributions of both methane and ozone (IPCC, 1995). The tools employed initially were zonally-averaged two-dimensional chemistry-transport models which treated only altitude-latitude variations in trace gas distributions and the processes which drive them. A discussion of the problems and concerns inherent in the application of zonally-averaged models for the quantitative representation of tropospheric ozone production and destruction is given in Johnson and Derwent (1996).

In this study, we have employed a global three-dimensional (altitude-latitude-longitude) Lagrangian chemistry-transport model (CTM) to study the transient behaviour of the tropospheric ozone precursor gases and have derived estimates for the magnitudes of their indirect greenhouse effects, based on their impacts on the tropospheric distributions of ozone and methane.

## 2. Description of the 3-D Lagrangian CTM

The model used in this study is the U.K. Meteorological Office tropospheric 3-D chemistry-transport model (STOCHEM). The STOCHEM model adopts a Lagrangian approach in which 50 000 constant mass air parcels are advected by winds from the Meteorological Office global circulation model. With this approach, all trace gas and aerosol species are advected simultaneously and the emission, chemistry, deposition and removal processes can be uncoupled from the advection.

### 2.1. ADVECTION AND DISPERSION PROCESSES

The Lagrangian air parcels were advected according to winds taken from the U.K. Meteorological Office Unified Model which is an operational numerical weather prediction model (Cullen, 1993) established on a grid of 1.25° longitude, 0.833° latitude and twelve unevenlyspaced vertical levels between the surface and about 100 mb. The advection timestep was set to three hours and new air parcel positions were calculated using a 4th order Runge–Kutta advection scheme. Winds were interpolated linearly in time within the 6-hourly meteorological datasets, bilinearly in the horizontal domain and using a cubic polynomial in the vertical.

Random displacements are added to the parcel velocities each time step based on globally constant diffusivities for the boundary layer, lower troposphere and upper troposphere. The treatment of small-scale convection utilised 6-hourly data covering the distribution of convective clouds. Interparcel exchange was described by relaxing the trace gas concentrations in an individual air parcel towards the mean concentration in adjacent air parcels.

### 2.2. CHEMISTRY

The three-dimensional model STOCHEM contains a full description of the photochemistry of the troposphere and the free radical reactions which process the emissions of the major tropospheric trace gases and ozone precursors. The representation of atmospheric chemistry includes 70 chemical species and 160 gas phase chemical reactions describing the chemistry of methane, $NO_x$, CO, $H_2$, $O_3$ and 11 emitted non-methane hydrocarbons. A chemistry timestep of 5 minutes is employed throughout day and night in the iterative backwards-Euler numerical integration routine. A full treatment of cloud processes has also been included to describe the uptake into cloud water of the gaseous species: $SO_2$, nitric acid, ozone, hydrogen peroxide and $NH_3$, together with their subsequent chemistry and wet scavenging.

A complete listing of the chemical mechanism with the selected rate coefficients, quantum yields and absorption cross sections based on literature data evaluations (Atkinson, 1994; Atkinson et al., 1996; DeMore et al., 1997) is available elsewhere (Collins et al., 1997, 1999). Photolysis rates were calculated every 45 minutes and values for each time-step were obtained by linear interpolation. Scavenging coefficients for large-scale and convective precipitation were adopted from Penner et al. (1994) and the scheme to convert fractional scavenging rates to grid cell average rates follows that of Walton et al. (1988). Dry deposition of $NO_2$, $SO_2$, CO, $O_3$, $HNO_3$, $H_2O_2$, $H_2$, $CH_3OOH$ and PAN to land and ocean surfaces have been described using a dry deposition velocity approach and the details are given elsewhere (Collins et al., 1997).

### 2.3. TREATMENT OF EMISSIONS

Emissions into the model were implemented as an additional term in the production flux for each species during each integration time-step. The emissions used are listed in Table I. The industrial, biomass burning, vegetation, soil, oceans and ‘other’ are all surface sources based on two-dimensional (latitude, longitude) source maps taken from the EDGAR database (Olivier et al., 1996). Aircraft $NO_x$ emissions were added using NASA inventories for 1992 (IPCC, 1999). The aircraft and lightning $NO_x$ sources are three-dimensional. The man-made and ‘other animal’ sources (see Table I) were held constant throughout the year at the yearly average value. The other sources varied by calendar month, with biomass burning redistributed with monthly fields from Cooke and Wilson (1996).

TABLE I
Model emissions in Tg $yr^{-1}$ [a,d]

| Species | Industrial | Biomass burning | Vegetation | Soil | Oceans | Other [b] |
|---|---|---|---|---|---|---|
| $NO_x$ [e] | 26.6 | 7.1 | | 5.6 | | |
| $SO_2$ | 72.8 | 1.6 | | | | |
| $H_2$ | 20.0 | 20.0 | | 5.0 | 5.0 | |
| CO | 684.0 | 700.0 | 150.0 | | 50.0 | |
| $CH_4$ | 308.9 | 15.3 | | | | 260.0 |
| $C_2H_4$ | 8.0 | 7.1 | 20.0 | | | |
| $C_2H_6$ | 7.0 | 3.6 | 3.5 | | | |
| $C_3H_6$ | 10.9 | 8.2 | 20.0 | | | |
| $C_3H_8$ | 7.3 | 1.0 | 3.5 | | 0.5 | |
| $C_4H_{10}$ | 63.1 | 2.1 | 8.0 | | | |
| $C_5H_8$ | | | 500.0 | | | |
| $C_8H_{10}$ | 9.9 | 1.1 | | | | |
| $C_7H_8$ | 9.8 | | | | | |
| $H_2CO$ | 1.6 | 1.3 | | | | |
| $CH_3CHO$ | 3.5 | 4.0 | | | | |
| Acetone [c] | 2.9 | 0.5 | 25.8 | | | |
| DMS | | | | | 26.1 | |
| $NH_3$ | 39.3 | 3.5 | | 2.4 | 8.1 | |

[a] Emissions are in Tg $yr^{-1}$ except for $NO_x$ which are in Tg N $yr^{-1}$.
[b] Includes paddies, tundra, wetlands, termites and animals.
[c] Acetone source from vegetation represents production from terpene oxidation.
[d] Emission totals and their spatial distributions were based on entries in the EDGAR database (Olivier et al., 1996).
[e] Aircraft $NO_x$ emissions for 1992 were taken from IPCC (1999).

In the STOCHEM model, surface emissions were added on a $5^\circ \times 5^\circ$ grid square basis. This is too coarse (600 km $\times$ 400 km at midlatitudes) to resolve individual centres of pollution but is large enough to resolve the heavily industrialised regions of Europe, Asia and North America and the biomass burning regions of Indonesia, Africa and South America. Stratospheric sources of ozone and nitric acid are calculated as two-dimensional inputs into the top model layer and varied on a 6-hourly basis. Averaged over each year there is a total ozone flux into the model domain of 865 Tg and a $NO_y$ flux of one thousandth of the ozone flux by mass (as N), based on the study of Murphy and Fahey (1994). No changes were made to the stratospheric sources in the perturbations described below.

## 2.4. MODEL VALIDATION

The concentrations of a wide range of tropospheric trace gases predicted by the STOCHEM model have been extensively compared with observations. Collins et al. (1997) describe a detailed comparison of STOCHEM results with surface ozone and ozonesonde observations. Collins et al. (1997) also compare model $NO_x$ results with observations for the middle troposphere. Collins et al. (1999) extend these comparisons to OH, $HO_2$, $H_2O_2$, $CH_3OOH$, HCHO and acetone. Collins et al. (2000) provide a detailed comparison of the surface ozone observations over Europe with STOCHEM results. The Lagrangian transport scheme has been extensively compared against an Eulerian scheme using $^{222}Rn$ as an inert and short-lived tracer (Stevenson et al., 1998).

Results obtained with the STOCHEM model have also been assessed and evaluated in a number of international model intercomparison exercises. These have included an evaluation of fast tropospheric photochemistry PHOTOCOMP (Olson et al., 1997), the GIM/IGAC intercomparison of model and observed $O_3$ distributions (Kanakidou, 1998), the GIM/IGAC intercomparison of model and observed CO distributions (Kanakidou, 1999) and the assessment of the impacts of subsonic aircraft $NO_x$ emissions on tropospheric ozone carried out within IPCC (1999).

Currently, there are not enough *in situ* measurements of hydroxyl radical concentrations with which to validate global chemistry-transport models. However, a measure of the magnitude of the global tropospheric distribution of hydroxyl radicals can be defined from observations of methane and methyl chloroform, trace gases whose main sink is chemical destruction by hydroxyl radicals. IPCC (1996) recommend a turn-over time for methane of $9.9 \pm 1.8$ years due to hydroxyl radical oxidation. The base case STOCHEM model gave 9.1 years for this turn-over time, in good agreement with the IPCC (1996) recommendation. The ratio of the turn-over times due to OH oxidation for methane relative to methyl chloroform is found to be 1.55 in the base case, leading to a methyl chloform turn-over time of 5.9 years due to this removal process. This is in good agreement with the determination of $5.4 \pm 1.0$ years due to OH oxidation estimated from observations (Prinn et al., 1995).

Furthermore, IPCC (1996) stress the importance of the concept of the methane adjustment time for which they report a value of $12.2 \pm 3$ years. The difference between the methane turn-over time and adjustment time thus amounts to a factor of 1.23 and this difference is the subject of the present study. The methane adjustment time found with STOCHEM is 12.3 years in good agreement with the IPCC (1996) recommendation above.

## 3. Description of the Transient Behaviour of the Tropospheric Ozone Precursors

### 3.1. MODEL STUDY OF THE TRANSIENT BEHAVIOUR OF METHANE

The transient behaviour of methane was investigated using the Lagrangian CTM model STOCHEM by starting the model from an initial set of trace gas concentrations in October 1994 and using analysed wind fields to run the model through to 1 January 1995. At that point, two model experiments were initiated. The first model experiment continued on from the previous annual cycle without change until 31 December 1998 and this formed the base case. In the second model experiment, the transient case, the methane emission source strength was increased so that a pulse containing an additional 40 Tg of methane was emitted into the model by 31 January 1995. At this point, the methane emission was reset to the base case value and the model experiment was continued until 31 December 1998. The impacts of the additional methane on the composition of the model troposphere were followed by taking differences between the base and transient cases. These differences in composition between the two experiments were termed 'excess' concentrations.

A diagrammatic representation of the base and transient case experiments is given in Figure 1 and follows in detail the impact of an emission pulse of methane on the composition of the model troposphere. Figure 1a presents the globally-integrated methane emissions over the four year's experiment, showing the pulse of the additional methane emissions during January 1995. Figure 1b shows the difference in globally-integrated methane loss rates between the two model experiments and the development of a small systematic difference or 'excess' between them following the pulse in methane emissions. The reaction of methane ($CH_4$) with hydroxyl radicals (OH) is the main loss process for methane and Figure 1b presents the globally-integrated 'excess' flux through the $OH + CH_4$ reaction.

As a result of the methane emission pulse (Figure 1a) and the difference in methane loss rates (Figure 1b), the methane burdens in the two model experiments begin to diverge.

The global methane burdens in both model experiments are plotted in Figure 1c and a small divergence becomes apparent between the transient experiment compared with the base case. The extra $OH + CH_4$ reaction flux then leads to reduced hydroxyl radical concentrations, see Figure 1d, in the transient experiment and this is shown as a negative 'excess' or 'deficit'. Because hydroxyl radical concentrations are reduced in the transient experiment, carbon monoxide (CO) concentrations build-up relative to the base case and an 'excess' CO accumulated, see Figure 1e. The increased $OH + CH_4$ reaction flux stimulated increased ozone production and an 'excess' ozone accumulated, see Figure 1f.

No special significance should be attributed to the choices of the magnitude, timing and spatial distribution of the methane emission pulse. The magnitude of

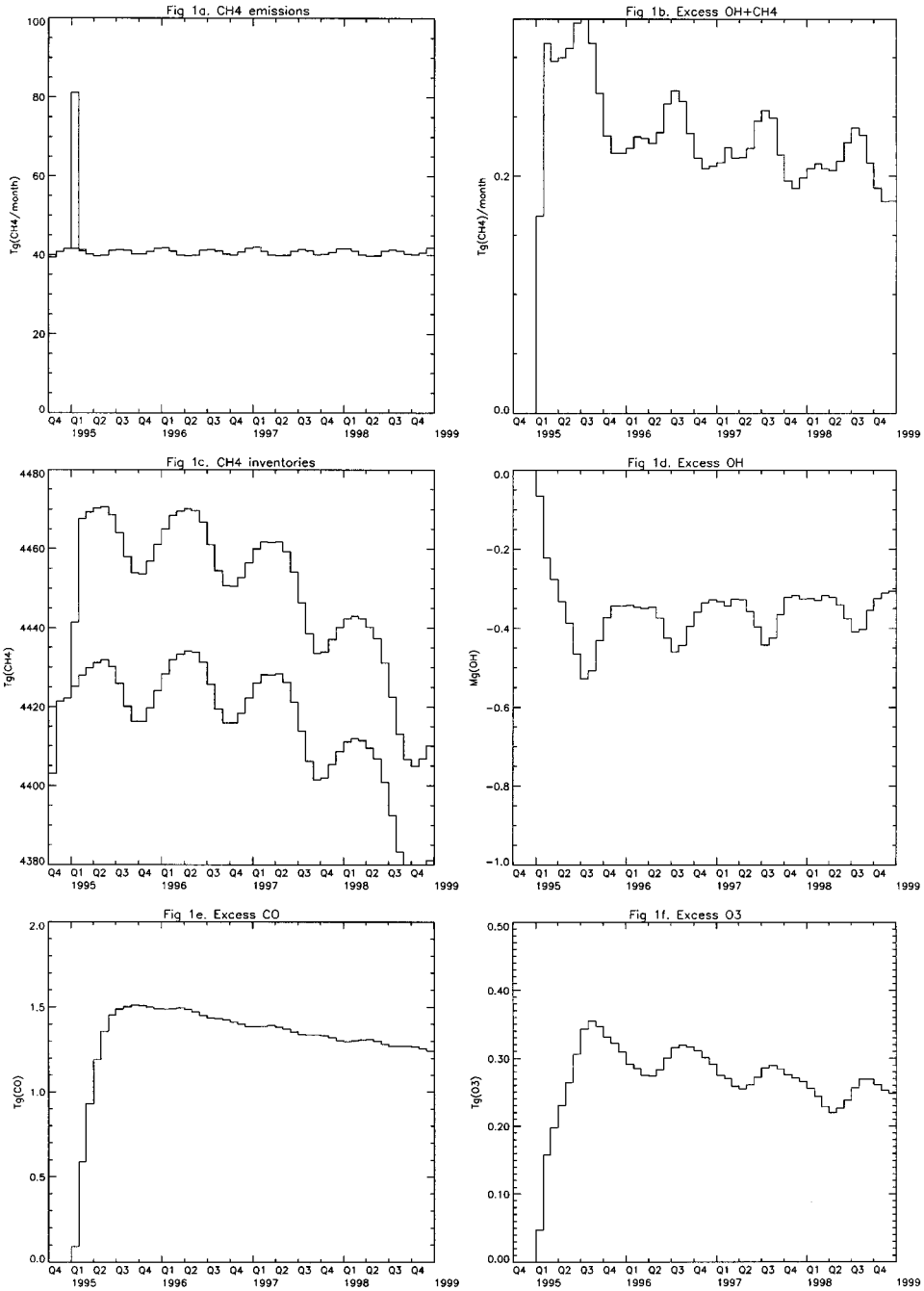


*Figure 1.* Diagrammatic representation of the effect of an emission pulse of methane on tropospheric composition showing (a) methane emissions in the base case (lower curve) and transient case (upper curve), (b) the 'excess' loss of methane through the OH + $CH_4$ reaction, (c) its tropospheric burden in the base case (lower curve) and transient case (upper curve), (d) the 'excess' OH radical burden, (e) the 'excess' CO burden and (f) the 'excess' tropospheric ozone burden.

the emission pulse in this and in the other model experiments was chosen to lie in the range between the monthly and annual emission rates and was small enough so that its influence on tropospheric composition was minimal but large enough so that the changes in the tropospheric distributions of OH, methane and ozone were detectable and of the order of a few percentage points. In any case, all the results were normalised to 1 Tg emission pulse subsequently. Some experiments were performed with the 2-D CTM described in our previous study (Johnson and Derwent, 1996) using emission pulses which were an order of magnitude larger to check linearity (methane: 53–653 Tg, CO: 29–263 Tg and $NO_x$: 0.9–16 Tg) and this was always seen. The emission pulses were distributed with the same spatial distribution as that of human population and industrial activity in Table I, based usually on fuel combustion or fuel handling statistics. No attempt was made to study comprehensively the impact of the many radically different spatial distributions which have already been adopted in the 3-D CTM or to study the impacts of particular continents or countries. Furthermore, any combination of time periods could have been chosen in which to emit the methane pulse but January was chosen solely to give the longest study period within the database of analysed wind-fields available.

Attention is directed at first to the methane response to the methane emission pulse, see Figure 1c. The 'excess' methane showed an abrupt rise to a maximum, followed by a slow decline which was incomplete at the end of the fourth year of the model experiment. During the first year of the model experiment, despite the 40 Tg or 0.9% increase in the methane burden in the transient experiment, the flux through the $OH + CH_4$ reaction increased by only 0.8%. Over the entire four year's model experiment, the methane turn-over time (global burden/removal rate) was 9.1 years in the base case whereas the turnover time of the 'excess' methane, defined as the 'excess' methane burden divided by the 'excess' methane loss rate or $\Delta(CH_4)/\Delta(OH + CH_4)$ was found to be significantly longer at 12 years. From the decay of the 'excess' methane burden over this same period, see Figure 1c, an e-folding time of 12.3 years was estimated, close to the average turnover time of the 'excess' methane.

The presence of the 'excess' methane in the transient case, see Figure 1c, led to a reduction in the hydroxyl radical concentrations relative to the base case due to the reaction sequence:

$$OH + CH_4 = CH_3 + H_2O$$
$$CH_3 + O_2 + M + CH_3O_2 + M\,.$$

Figure 1d shows how this depletion of the hydroxyl radical burden or negative 'excess' built up in the transient case, reaching a maximum six months after the start of the model experiment. Because of the depletion in the hydroxyl radical concentrations in the transient case, the $OH + CH_4$ reaction flux did not increase in step with the methane burden to maintain the same turnover time in both experiments. Without this depletion effect, the turnover time of the 'excess' methane would be

the same as that in the base case model. This depletion of hydroxyl radicals is caused by the subsequent reactions of the methylperoxy ($CH_3O_2$) radicals.

The 'excess' methane decays with a longer e-folding time (12.3 years) than expected from the steady state turnover time (9.1 years) and hence a methane pulse persists longer in the troposphere than would be expected. That is to say, the methane adjustment time in the 3-D CTM is significantly longer than than the atmospheric turnover time as determined from its global burden and steady state removal rate. That methane concentrations remain elevated longer than expected following an emission pulse has sometimes been referred to as the methane self-feedback or self-poisoning effect. These higher concentrations lead to higher than expected radiative forcings, with the differences being termed the indirect methane radiative forcing. The adjustment time found here of 12.3 years is in excellent agreement with the value assessed by the Intergovernmental Panel on Climate Change of $12.2 \pm 3$ years (IPCC, 1996).

### 3.2. THE IMPACT OF OTHER TROPOSPHERIC OZONE PRECURSORS ON METHANE

A series of model experiments were then performed in which the methane emission pulse was substituted by a corresponding pulse of other ozone precursor species: carbon monoxide (CO), oxides of nitrogen ($NO_x$) and hydrogen. The methane transient responses which were driven by emission pulses of a range of ozone precursor species are each characteristically different, see Figure 2. In this Figure, the model responses have been normalised by the magnitude of the emission pulses studied to give responses for a 1 Tg emission pulse of each species. In our previous work with a 2-D CTM, we used step-changes in emissions rather than emission pulses because the former model was computational efficient enough to allow model experiments covering up to 100 years. In the present study with a 3-D CTM which is several orders of magnitude more computationally intensive, model experiments have extended only over 4 years and so emission pulses have been simulated because of their simpler theoretical interpretation.

Figure 2 confirms that all of the ozone precursor species can individually stimulate changes in the methane concentration distribution in response to a pulse in their emissions. Pulses in carbon monoxide and hydrogen, in addition to methane, produce increases in methane concentrations through depletion of hydroxyl radicals through the reactions:

$$\mathrm{OH} + \mathrm{CO} = \mathrm{H} + \mathrm{CO_2}$$
$$\mathrm{OH} + \mathrm{H_2} = \mathrm{H_2O} + \mathrm{H}\,.$$

In contrast, pulses in $NO_x$ emissions produce decreases in methane concentrations through stimulation of hydroxyl radical production through the reaction:

$$\mathrm{NO} + \mathrm{HO_2} = \mathrm{NO_2} + \mathrm{OH}\,.$$

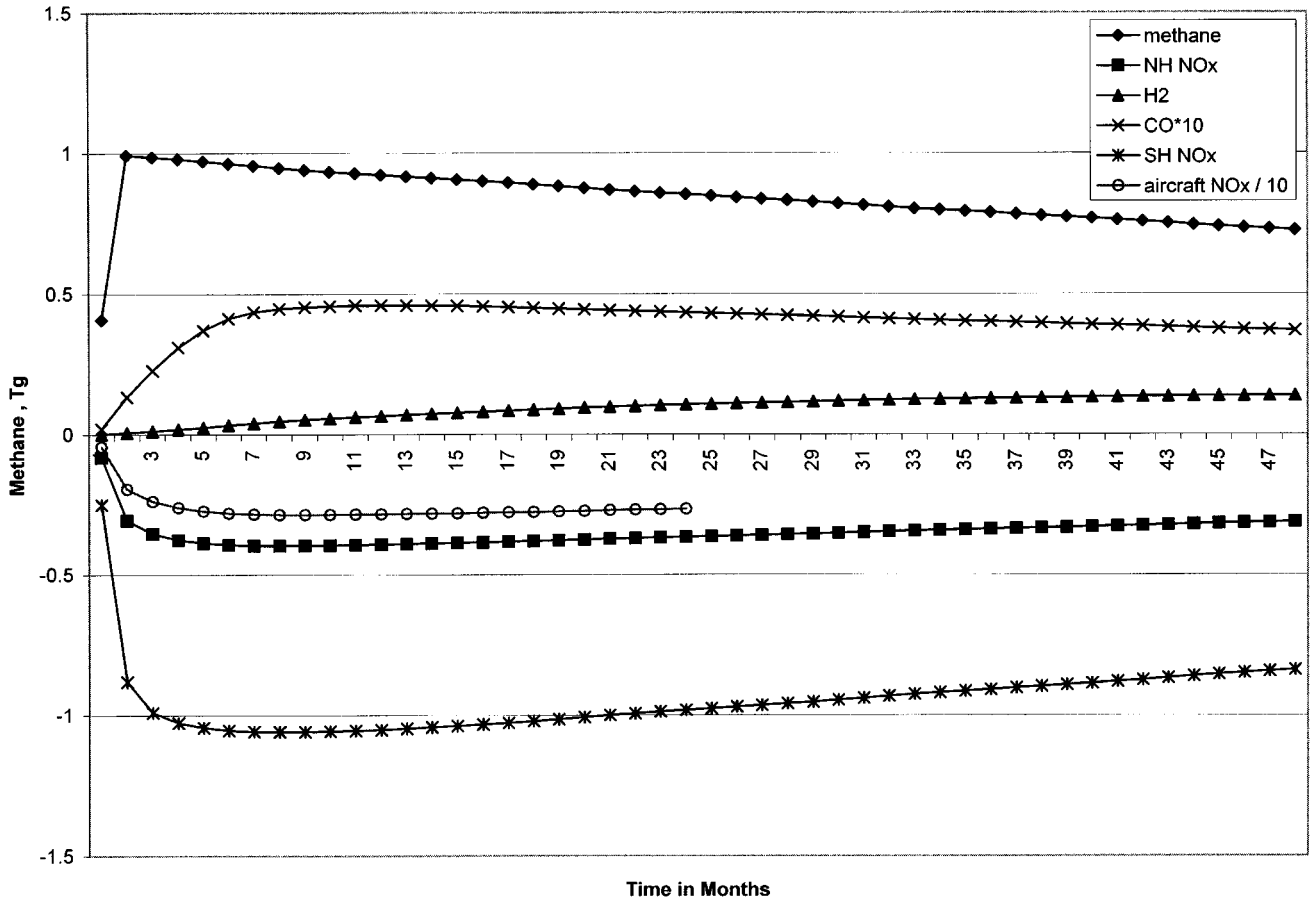


*Figure 2.* A summary of the methane responses to emission pulses of the different tropospheric ozone precursors normalised to a 1 Tg emission pulse.

In Figure 2, the methane responses have been normalised to a 1 Tg pulse by dividing by the magnitude of the emission pulse actually employed in each STOCHEM experiment. On this normalised basis, pulses in $NO_x$ appear to exert a greater influence on methane compared with the other ozone precursors and aircraft $NO_x$ emissions significantly greater than surface $NO_x$ emissions. Figure 2 confirms earlier 2-D model studies (Johnson and Derwent, 1996) which demonstrated similar differences in methane responses to step-changes in $NO_x$ emissions.

In each case in Figure 2, the methane response increases towards its maximum 'excess' or 'deficit' before a steady decline sets in for the remainder of the experiment. Although the initial behaviour differs significantly between the different ozone precursors, the decay phases look strikingly similar. Indeed, each curve exhibits a similar e-folding time of about 12 years. Detailed analysis is hampered by the limited experimental period used because of the computational burden involved with the 3-D CTM. Nevertheless, the experimental period is long enough to show that e-folding times for the decay of the methane responses are in every case significantly longer than methane lifetimes. There is therefore a significant indirect impact on the tropospheric methane distribution from the emission pulses of all of the ozone precursors.

We have also set up these identical pulse experiments in the 2-D CTM employed in our previous investigation (Johnson and Derwent, 1996) and followed each pulse for 20 years. The mean e-folding time for methane found during 18 2-D CTM experiments covering methane, CO, $NO_x$, $H_2$ and a range of hydrocarbons was $12.0 \pm 0.7$ years. This confirms the view obtained from the 3-D CTM that, regardless of the initial response to the pulse, all the methane responses ultimately settle down and decay with an identical e-folding time of about 12 years, a timescale which is significantly longer than the methane steady state lifetime, defined as the global burden divided by the steady state loss rate.

On this basis then, Table II presents the time-integrated methane excess or deficit for each tropospheric ozone precursor gas, obtained by taking the 3-D CTM methane 'excess' or 'deficit' after four years and extrapolating its decay over a 100-year time horizon using the observed e-folding time. In each case, the methane response has been normalised by the magnitude of the emission pulse and expressed on a 1 Tg basis. Time-integrated methane 'excesses' have been determined for methane, CO, $H_2$, and $NO_x$ emissions. Irrespective of sign, time-integrated methane responses appear to be largest for aircraft and surface southern hemisphere $NO_x$ emission pulses.

### 3.3. THE EFFECTS OF THE TROPOSPHERIC OZONE PRECURSORS ON THE OZONE DISTRIBUTION

As a result of the increase in the concentrations of each tropospheric ozone precursor species following its emission pulse, adjustments followed in the concentrations of the major tropospheric free radical species and ultimately in tropospheric

TABLE II

Methane responses to emission pulses of a range of tropospheric ozone precursor species, integrated over a 100-year time horizon, expressed in terms of concentrations and radiative forcing [a]

| Tropospheric ozone precursor | Methane response, ppb years | Radiative forcing, mW $m^{-2}$ years |
|---|---|---|
| Methane | 4.8 | 2.1 |
| Surface $NO_x$ in NH | –2.1 | –0.9 |
| Surface $NO_x$ in SH | –5.8 | –2.5 |
| Aircraft $NO_x$ | –15.9 | –6.9 |
| Carbon monoxide | 0.25 | 0.11 |
| Hydrogen | 0.81 | 0.35 |

[a] Each methane response has been normalised to an emission pulse of 1 Tg (as $CH_4$, $NO_x$, CO and $H_2$).

ozone. For all of the ozone precursor species studied, ozone production was stimulated so that by the end of each four-year model experiment, net increases in tropospheric ozone could be discerned. Figure 3 illustrates the ozone responses, integrated up to the top of the 3-D CTM at 16 km and from pole-to-pole, that were found for each tropospheric ozone precursor species, normalised by the emission pulse on a 1 Tg basis.

The ozone responses in Figure 3 show characteristically different behaviour for each of the ozone precursor species studied. The responses to the $NO_x$ and CO pulses show a steep rise followed by a steep decay whereas the responses to the methane and hydrogen pulses show a steady increase followed by a steady decline. On a normalised basis, the $NO_x$ responses are huge in comparison to all of the others (note: the methane, carbon monoxide and hydrogen responses in Figure 3 have been scaled by 100 so that they appear in the same plotting region). There appears to be no uniformity in the steepness of the decays of the ozone responses across the range of trace gases studied. This is in direct contrast to the distinct uniformity found with the decays in the methane responses. However, it was apparent that ultimately the ozone response to the methane pulse decayed away with an e-folding time of 12 years, exactly the same as that found for the ‘excess’ methane in that same experiment.

To examine further the long-term nature of the ozone responses well after the initial phase of the ozone responses, Figure 4 plots the decays of the ‘excess’ ozone concentrations on a logarithmic scale against time after the emission pulse. Here we have taken the global average of the excess ozone concentrations in the upper troposphere, corresponding to the 500–200 mb pressure range, 4.2–11.8 km altitude range. After the initial reponse which is more clearly defined in Figure 3, the logarithm of the ozone concentrations decline linearly with similar slopes for

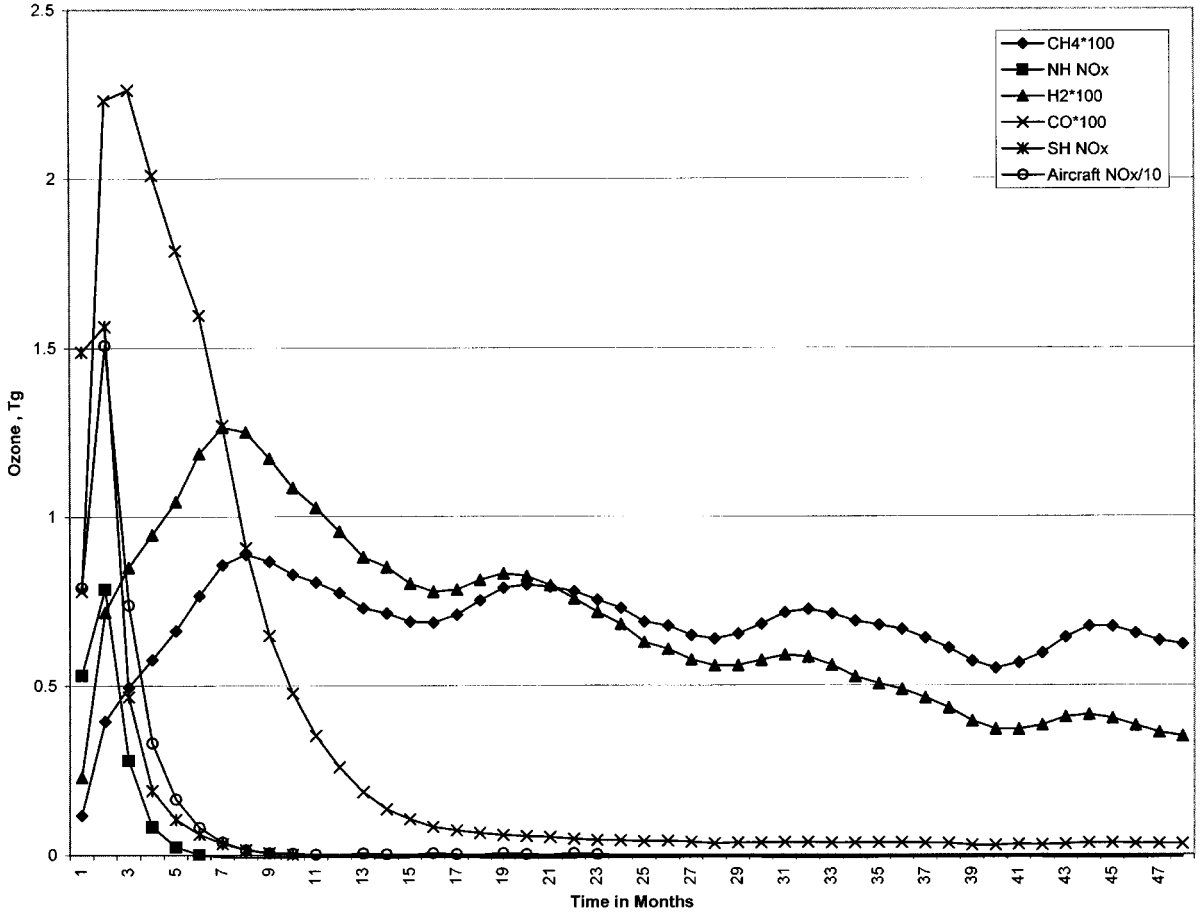


*Figure 3.* A summary of the tropospheric ozone responses to emission pulses of the different tropospheric ozone precursors normalised to a 1 Tg emission pulse.

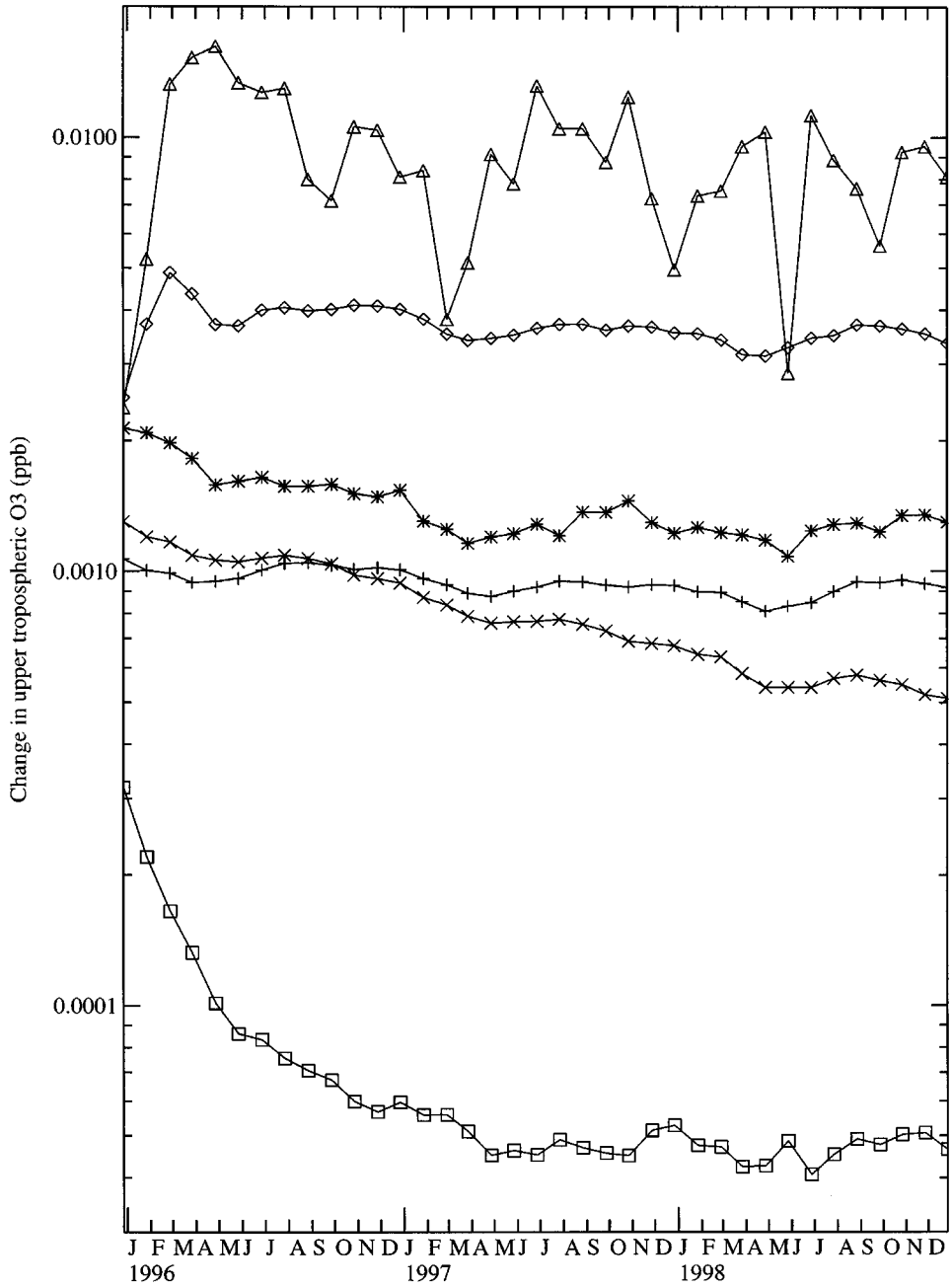


*Figure 4.* A summary of the upper tropospheric ozone concentration responses to emission pulses of the different tropospheric ozone precursors, plotted with a logarithmic scale. Key: + 40 Tg methane, ∗ 6.6 Tg $NO_x$ global, ◇ 6.6 Tg $NO_x$ southern hemisphere, △ 0.13 Tg $NO_x$ aircraft, squares 40 Tg carbon monoxide and × 40 Tg hydrogen.

TABLE III

Tropospheric ozone response to emission pulses of a range of tropospheric ozone precursor species, integrated over a 100-year time horizon, expressed in terms of concentrations and radiative forcing

| Tropospheric ozone precursor | Ozone response,[a] ppb years | Radiative forcing, mW $m^{-2}$ years |
|---|---|---|
| $CH_4$ | 0.015 | 0.34 |
| Surface $NO_x$ in NH | 0.021 | 1.4 |
| Surface $NO_x$ in SH | 0.045 | 4.1 |
| Aircraft $NO_x$ | 0.52 | 36.0 |
| CO | 0.002 | 0.06 |
| $H_2$ | 0.01 | 0.25 |

[a] Each ozone response has been normalised to an emission pulse of 1 Tg (as $CH_4$, $NO_x$, CO and $H_2$).

each tropospheric ozone precursor gas, see Figure 4. These limiting slopes after the first year correspond to e-folding time constants of about 12 years as found for the 'excess' ozone in the methane experiment. The only exception in Figure 4 appears to be in the experiment with the emission pulse of hydrogen. Here the 'excess' ozone decays much more steeply across the first three years of the four-year period (crosses in Figure 4). This behaviour is consistent with an initial ozone response which takes three years to decay away, leaving the 'excess' ozone to decay away in the final year with an e-folding time of 12 years, exactly as found in the remainder of the experiments.

The above conclusions from the 3-D CTM were confirmed by running the 2-D CTM employed in our previous study (Johnson and Derwent, 1996). Over a series of 18 model experiments covering 20 years and studying a range of ozone precursors, ozone responses initially decayed with e-folding times which varied from 100 days (for toluene) to 12 years (for methane) before finally settling down with an e-folding time of 12 years. Thus, the e-folding times for the methane and ozone responses to the methane pulse were found to be identical at 12 years in both the 3-D and 2-D CTMs. The results from the 3-D CTM studies appear not to have been overly influenced by the short experimental periods employed and agree closely with those from the 2-D CTM.

Table III presents the time-integrated ozone concentration responses, over a 100-year time horizon, to emission pulses in each of the ozone precursor species. These time-integrated concentrations have been estimated by taking the ozone response after 4 years and extrapolating over 100 years using the e-folding time of the ozone decay found in each experiment. The ozone concentration changes have been taken from the 3-D CTM model covering 500–200 mb (4.2–11.8 km range) and averaged from pole-to-pole. This altitude range includes the layers where ozone

changes exhibit their greatest radiative forcing impact (Lacis et al., 1990). The normalised time-integrated ozone concentrations appeared to be significantly greater for the $NO_x$ emission pulses compared with those of the other ozone precursors.

### 3.4. COMPARISON OF THE TRANSIENT BEHAVIOUR IN THE 3-D CTM WITH THEORY

From a consideration of the lifetimes and eigenstates of a simplified one-box representation of the tropospheric $CH_4$–CO–OH system, Prather (1994) has predicted that the longest time constant of that system would always be longer than the steady state turnover time of methane. This lengthening of the recovery time from a methane, CO or OH perturbation was seen as a diagnostic for the chemical stability of the troposphere (Prather, 1994). This apparent lengthening of the methane response to perturbations has been carefully taken into account in quantifying the radiative forcing consequences of methane emissions (IPCC, 1995).

Using the STOCHEM 3-D CTM, we have shown that methane perturbations decay more slowly than expected from its steady state turnover time. Furthermore, the methane adjustment times have been shown here to be independent of the trace gas chosen to produce the initial perturbation. These observations of the transient behaviour provide striking confirmation of the theoretical predictions of Prather (1994). We show here how the methane adjustment time is 1.35 times longer than the steady state methane turnover time. The corresponding factor for the simplified one-box model of Prather (1994) was about 1.6 with a rather wide uncertainty range from 1–2.

Furthermore, we have examined the transient behaviour of a wide range of trace gases in these same model runs. We have found that, after a long enough time, all the time constants settle down to the same exponential decay as characterised by the methane adjustment time. This is the case in particular for upper tropospheric ozone and the trace gases controlled by the distribution of tropospheric hydroxyl radicals.

The global one-box model adopted by Prather (1994) contains a number of simplifications and assumptions which were recognised and discussed fully. Our experience has shown just how realistic its predictions are compared with those from a 3-D CTM. Quantitatively the 3-D CTM behaves as if it is further displaced from the position of chemical instability compared with the global one-box model. That is to say, OH appears to be in larger excess than assumed by Prather (1994) in his base case. This necessarily reduces the magnitude of the difference between the adjustment time and the steady state turnover time as discussed above. It may well be that there are transients in other species such as hydrogen with intermediate lifetimes which have been neglected by Prather (1994) but which have been treated in the 3-D model and these could explain the relative displacements of the two models. It will take further work to establish whether the global one-box or the 3-D CTM are closer to the real troposphere.

## 4. Radiative Forcing and Global Warming Potentials

Using the radiative forcing formulae for methane laid out by IPCC (1990) the time-integrated 'excess' methane concentrations in Table II were converted into time-integrated radiative forcing, over a 100-year time horizon. On this basis, for example, a 1 Tg emission pulse of methane produced a time-integrated methane radiative forcing of 2.1 mW $m^{-2}$ year over a 100-year time horizon, see Table II.

To estimate the radiative forcing consequences of the tropospheric ozone changes found in the 3-D CTM we employed the Edwards and Slingo (1998) radiation code at low spectral resolution. Clouds and temperatures were represented using the meteorological archives driving the 3-D CTM. Stratospheric temperatures were iteratively adjusted until stratospheric heating rates returned to their unperturbed values and details of the methodology are given elsewhere (Stevenson et al., 1998). The radiative forcing caused by the differences between the transient and base cases were calculated for each month of the second year of the methane experiment. This radiative forcing showed a slight seasonal cycle during this year which reached a minimum of 0.86 mW $m^{-2}$ in January and increased to a maximum in July of 1.04 mW $m^{-2}$. This corresponded to a radiative forcing of 0.023 W $m^{-2}$ per ppb change in the global mean ozone concentration in the 4.8–11.2 km, 500–200 mb altitude range. In estimating the time-integrated ozone radiative forcing in Table III, it was assumed that radiative forcing was linear in ozone change in the upper troposphere and that the second year of the methane experiment could be used to define this implied relationship for all the model experiments. On this basis, a 1 Tg emission pulse of methane produced a time-integrated ozone radiative forcing of 0.34 mW $m^{-2}$ years over a 100-year time horizon.

The tropospheric ozone precursors which are derived from fossil-carbon will ultimately generate additional carbon dioxide as they degrade in the atmosphere. This consideration applies particularly to carbon monoxide and methane. An assessment of the radiative consequences of an emission pulse of fossil carbon monoxide or of fossil methane should include an assessment of the impact of the $CO_2$ formed by atmospheric degradation. The 3-D CTM provides the relevant information on the time dependent production of $CO_2$ following the emission pulse. The fate of this $CO_2$ was described using the $CO_2$ response function of the Bern carbon cycle model (IPCC, 1996) run for a constant mixing ratio of $CO_2$ over a 500-year period. On this basis, a 1 Tg emission pulse of fossil methane produced a time-integrated excess $CO_2$ concentration of 14.5 ppb years over a 100-year time horizon. Using the radiative forcing formula in IPCC (1990), this emission pulse generated a time-integrated radiative forcing of 0.25 mW $m^{-2}$ years.

The time-integrated radiative forcing estimates for the different forcing mechanisms and for the different tropospheric ozone precursors are brought together in Table IV. These time-integrated radiative forcings can be converted into global warming potentials by comparison with the time-integrated forcing of a reference gas, usually taken to be $CO_2$. Here, we define the Global Warming Potentials GWP

TABLE IV

Global warming potentials for three radiative forcing mechanisms for a range of different emission pulses of tropospheric ozone precursor species over a 100-year time horizon[a]

| Tropospheric ozone precursor | GWP from changes to methane | GWP from changes to ozone | GWP from changes to $CO_2$ |
|---|---|---|---|
| $CH_4$ | 20.0 | 3.3 | 2.4 |
| Surface $NO_x$ in NH | –8.5 | 13 | |
| Surface $NO_x$ in SH | –24.0 | 39 | |
| Aircraft $NO_x$ | –65.9 | 343 | |
| CO | 1.0 | 0.6 | 1.6 |
| $H_2$ | 3.4 | 2.4 | |

[a] Each GWP has been expressed relative to an emission pulse of 1 Tg (as $CH_4$, $NO_x$, CO, $CO_2$ and $H_2$).

of a tropospheric ozone precursor as the ratio of the time-integrated radiative forcing for a particular radiative forcing mechanism resulting from the emission of a pulse of 1 Tg of that species compared with that from the emission of 1 Tg (as $CO_2$) of $CO_2$ over a hundred year time horizon.

The Global Warming Potentials of the tropospheric ozone precursors are given in Table IV. The highest GWP values are found for the $NO_x$ emissions generally, with aircraft $NO_x$ emissions showing the highest values. For $NO_x$ emissions, ozone and methane radiative forcings have opposite signs whereas for the other tropospheric ozone precursors, these forcing mechanisms reinforce each other. In general terms, the indirect ozone and methane radiative forcing mechanisms are not negligible for any of the tropospheric ozone precursors and any comprehensive treatment of radiative forcing from methane and ozone will need to take into account the joint influence of a wide range of tropospheric ozone precursors. A further conclusion is that the GWPs of the tropospheric ozone precursors appear to be markedly dependent on the location of the emission pulse as indicated by the differences between the entries in Table IV for aircraft and surface $NO_x$ emissions, for example.

In Table IV, the GWPs are compared for a range of different emission pulses for the methane and ozone radiative forcing mechanisms. The $GWP^{CH_4}$ values for the three different $NO_x$ emission pulses were all strongly negative whereas the values for $CH_4$, CO and $H_2$ were positive. These differences reflect the overriding importance of the $NO + HO_2$ reaction which acts to increase OH concentrations, to decrease methane build-up and hence decrease methane radiative forcing. The variation of $GWP^{CH_4}$ for the different $NO_x$ emission pulses reflects the influence of $NO_x$ background levels. The lower the background $NO_x$ levels, the more negative the $GWP^{CH_4}$ values. The $GWP^{CH_4}$ is much higher than that for CO and $H_2$ because of the direct contribution to the $GWP^{CH_4}$ from methane itself. The $GWP^{CH_4}$ for

$H_2$ is much higher than that for CO although they have identical influences on tropospheric chemistry because the entries in that table have been made on a mass-emitted basis.

All of the tabulated $GWP^{O_3}$ values are positive showing that emission pulses of all of the compounds stimulate increased tropospheric ozone production. The $GWP^{O_3}$ values for $NO_x$ are the largest with highest values for pulses of emissions in those regions with the lowest background $NO_x$ levels. The $GWP^{O_3}$ values for $CH_4$, CO and $H_2$ expressed on a mass basis are heavily influenced by the low molecular mass of $H_2$. On a molar basis, the relative radiative forcing indices change order and become 4 : 14 : 53, respectively. The high value for methane reflects its higher ozone forming potential through the reactions of the $CH_3O_2$ and $HO_2$ radicals. Hydrogen appears to have much reduced potential because its tropospheric removal is not dominated by OH reaction as it is with $CH_4$ and CO because of the importance of soil uptake in its life cycle (Simmonds et al., 2000).

## 5. Discussion and Conclusions

In this study, 3-D CTM model calculations have been used to identify the likely magnitudes of the indirect radiative forcing impacts of emission pulses of the short-lived tropospheric ozone precursor species, through changes in the tropospheric distributions of methane and ozone. These radiative impacts have been expressed on a common basis using the Global Warming Potential GWP concept. That is to say the radiative forcing consequences of the emission of a 1 Tg pulse of each species have been compared to the consequences of emitting 1 Tg (as $CO_2$) of $CO_2$, integrating all radiative forcings over a 100-year time horizon.

For methane we report a GWP of 23.3 for methane and ozone forcing combined, over a 100-year time horizon which compares well with the WMO (1998) and the IPCC (1996) values of 24. There is an argument for not including the $CO_2$ formation term from fossil methane because of double-counting (WMO, 1998), however, under some policy circumstances, it is appropriate to add in the $CO_2$ formation term and hence its inclusion in Table IV for completeness. This study, in contrast to IPCC (1996) and WMO (1998), makes no evaluation of the radiative impact of stratospheric water formation. The current GWP value for methane is also in good agreement with the value of 28.7 that we have previously reported with our 2-D CTM (Johnson and Derwent, 1995) the discrepancy being accounted for by the differences between emission pulses (used here) and step-changes (used previously).

It is concluded that indirect radiative impacts make a substantial contribution to the radiative consequences of atmospheric methane emissions and their inclusion is therefore of paramount importance. The magnitudes of the methane self-feedback or indirect methane radiative forcing found in this study are well within the ranges covered by previous studies.

There are few reported determinations of the GWP for carbon monoxide in the literature. Daniel and Solomon (1998) have estimated a GWP of between 1–4 using a global box model. The value reported here of 1.5 is well within that range, disregarding the contribution from $CO_2$ formation. Previously we have reported a value of 2.1 (Johnson and Derwent, 1996) also in good agreement with the value in Table IV for step-changes in CO rather than emission pulses.

The GWPs reported here for $NO_x$ show significant differences from those we have reported previously using a 2-D CTM. The $GWP^{O_3}$ values for all $NO_x$ emission sources appear to be a factor of 1·5 smaller with the 3-D CTM compared with the 2-D CTM. Because of too coarse spatial resolution, 2-D models readily mix $NO_x$ into remote environments beyond their actual transport distances and stimulate ozone production in these $NO_x$-limited environments (Johnson and Derwent, 1996). Inadequacies in the 2-D models therefore presumably explain the differences between the 2-D and 3-D model results for $GWP^{O_3}$. The $GWP^{CH_4}$ values for surface $NO_x$ sources are in reasonable agreement and only that for aircraft emissions shows any significant difference between the 2-D and 3-D models. In this case, the 2-D model appears to understate the $GWP^{CH_4}$ by about a factor of two compared with the 3-D model. Here, the too coarse spatial resolution of the 2-D model appears to have dispersed the $NO_x$ from the air traffic corridor too efficiently and reduced its local influence on OH and hence on CO and $CH_4$.

An important feature of the GWPs reported in this study for surface $NO_x$ emissions are their marked geographical variations. Southern hemisphere injections appear to produce to a three-fold greater response from methane and ozone compared with corresponding northern hemisphere injections. Fuglestvedt et al. (1999) stopped short of calculating GWPs but they did report relative methane and ozone responses to step-changes in $NO_x$ emissions from different geographical regions. Methane responses appear to be higher by factors of 4–6 from southern hemisphere $NO_x$ emission reductions compared with similar reductions in northern hemisphere $NO_x$ emissions (Fuglestvedt et al., 1999). Ozone responses appear a factor of 2–4 greater from reductions in southern hemisphere $NO_x$ emissions compared with northern hemisphere emissions (Fuglestvedt et al., 1999). The geographical variations reported here are thus entirely consistent with those reported by Fuglestvedt et al. (1999).

As far as we are aware, this is the first reported determination of the GWP for hydrogen. Hydrogen is a candidate future fuel and is considered to have few environmental impacts. We have shown here that hydrogen, when emitted into the atmosphere, perturbs tropospheric hydroxyl radical distribution which can then lead to increased methane and ozone levels. Hydrogen emissions appear to generate an indirect radiative forcing in contradiction to the commonly held view that switching to hydrogen-based fuels will eliminate global warming.

In the past, the Intergovernmental Panel on Climate Change have deliberately not recommended relative radiative forcing indices, global warming potentials included, for any short-lived trace gas species and have only provided estimates for

well-mixed greenhouse gases (IPCC, 1996). There are a number of reasons why GWPs for short-lived trace gases have been considered uncertain and unreliable. The first and perhaps most important reason has been the lack of availability of state-of-the-art global 3-D model studies of the influence of short-lived trace gases on the fast photochemistry of the troposphere which controls the global distributions of methane and ozone. The second reason is that the influence of the short-lived trace gases is likely to be inherently more variable in space and time and that these variations would be difficult to express in a single number for a GWP.

Subsequently, a considerable number of global three-dimensional CTM models have been developed and applied to increase our understanding of the influence of short-lived trace gases on the distributions of methane and of tropospheric ozone. A sub-set of these 3-D CTMs have been used by IPCC (1999) to quantify the impact of aircraft $NO_x$ emissions on methane and tropospheric ozone. IPCC (1999) indicated a reasonable level of confidence in the results from state-of-the-art 3-D CTMs, sufficient to quantify the indirect radiative forcing indices for the methane and ozone impacts of subsonic aircraft $NO_x$ emissions. In this present study, one of the 3-D CTMs employed in the IPCC (1999) aircraft evaluation has been employed to determine indicative indirect radiative forcing indices for a wider range of trace gas emissions, other than aircraft $NO_x$ emissions.

Although it is felt that the 3-D CTM used here has addressed many of the shortcomings inherent in previous 2-D CTM studies, as discussed in detail elsewhere (Johnson and Derwent, 1996), questions still remain concerning the spatial and temporal variations in GWPs for short-lived trace gases. This study has considered only a very limited range of plausible locations and timescales for the emission pulses because of the computational demands of 3-D CTMs. Nevertheless in this initial study, we have shown that the GWP for $NO_x$ is distinctly different for an aircraft injection as opposed to a surface emission and that emissions in the northern and southern hemispheres are also different. Fuglestvedt et al. (1999) report different impacts from surface $NO_x$ emissions in Asia, America, Europe and Australasia. The different GWPs found here for different spatial patterns of changes in surface $NO_x$ emissions are entirely consistent with the different $NO_x$ sensitivity factors reported by Fuglestvedt et al. (1999).

On balance, our studies show that GWPs for short-lived trace gases are likely to be spatially and temporally variant. This study has begun the process of starting to quantify GWPs for the tropospheric ozone precursors by choosing one winter month to perform the emission pulse and by using previously published spatial patterns to define the spatial context. The aim is to steadily extend the coverage of the GWPs with further studies as understanding of tropospheric chemistry develops.

In Table V an attempt is made to consider what clues can be gleaned as to the relative importance for global warming of the emissions of tropospheric ozone precursor gases from human activities, using the GWPs calculated here. Looking first at the radiative forcing from the well-mixed greenhouse gas, methane, then

TABLE V

Global emissions of tropospheric ozone precursors from human activities weighted by their respective GWPs over a 100-year time horizon

| Tropospheric ozone precursor species | Fossil-fuel related emissions, Tg $yr^{-1}$ [a] | $GWP^{CH_4}$ weighted emissions, Tg $yr^{-1}$ | $GWP^{O_3}$ weighted emissions, Tg $yr^{-1}$ |
|---|---|---|---|
| $CH_4$ [b] | 100 | 2000 | 330 |
| Surface $NO_x$ [c] | 69 | –600 | 900 |
| Aircraft $NO_x$ [c] | 1.8 | –120 | 620 |
| CO | 425 | 425 | 220 |
| $H_2$ | 20 | 70 | 40 |

[a] Emissions from human population-based and industrial activities were taken from Table I, Collins et al. (1999) and Olivier et al. (1996).
[b] Fossil fuel related emissions for methane were taken from IPCC (1996).
[c] Emissions reported on $NO_x$ basis.

GWP-weighted emissions appear to be heavily dominated by emissions of methane itself, with those of surface $NO_x$ emissions a factor of three smaller. Then looking at the radiative forcing from tropospheric ozone which is more regional in character, all of the ozone precursor gases appear to be crucial in establishing the contribution to global warming. Although methane is considered within the scope of the Framework Convention on Climate Change, this is not the case for the other tropospheric ozone precursors. A case can be made for their inclusion in the Framework Convention alongside methane, if future methane and tropospheric ozone levels are to be stabilised and eventually reduced to combat global climate change. However, in view of the dependence of the GWPs presented here on where the ozone precursor gases are released and a host of other factors, it is concluded that this study is just the beginning of those needed for a detailed assessment of GWPs.

## Acknowledgements

This study was supported as part of the Public Meteorological Service R&D Programme of the Met Office and by the Department of the Environment, Transport and the Regions through contracts PECD 7/12/37 (Global Atmosphere Division) and EPG 1/3/143 (Air and Environmental Quality Division).

## References


Atkinson, R.: 1994, 'Gas-Phase Tropospheric Chemistry of Organic Compounds', *J. Phys. Chem. Ref. Data* **Monograph Number 2**, 1–216.

Atkinson, R., Baulch, D. L., Cox, R. A., Hampson, R. F., Kerr, J. A., Rossi, M. J., and Troe, J.: 1996, 'Evaluated Kinetic and Photochemical Data for Atmospheric Chemistry. Supplement V. IUPAC Subcommittee on Gas Kinetic Data Evaluation for Atmospheric Chemistry', *Atmos. Environ.* **30**, 3903–3904.

Collins, W. J., Stevenson, D. S., Johnson, C. E., and Derwent, R. G.: 1997, 'Tropospheric Ozone in a Global-Scale Three-Dimensional Lagrangian Model and its Response to $NO_x$ Emissions Controls', *J. Atmos. Chem.* **26**, 223–274.

Collins, W. J., Stevenson, D. S., Johnson, C. E., and Derwent, R. G. : 1999, 'The Role of Convection in Determining the Budget of Odd Hydrogen in the Upper Troposphere', *J. Geophys. Res.* **104**, 26927–26941.

Collins, W. J., Stevenson, D. S., Johnson, C. E., and Derwent, R. G.: 2000, 'The European Regional Ozone Distribution and its Links with the Global Scale for the Years 1992 and 2015', *Atmos. Environ.* **34**, 255–267.

Cooke, W. F. and Wilson, J. J. N.: 1996, 'A Global Black Carbon Aerosol Model', *J. Geophys. Res.* **101**, 19395–19409.

Crutzen, P. J.: 1974, 'Photochemical Reactions Initiated by and Influencing Ozone in the Unpolluted Troposphere', *Tellus* **26**, 47–57.

Cullen, M. J. P.: 1993, 'The Unified Forecast/Climate Model', *Met. Mag.* **122**, 8194, London, U.K.

Daniel, J. S. and Solomon, S.: 1998, 'On the Climate Forcing of Carbon Monoxide', *J. Geophys. Res.* **103**, 13249–13260.

DeMore, W. B., Sander, S. P., Golden, D. M., Hampson, R. F., Kurylo, M. J., Howard, C. J., Ravishankara, A. R., Kolb, C. E., and Molina, M. J.: 1997, *Chemical Kinetics and Photochemical Data for Use in Stratospheric Modeling*, Evaluation Number 12, JPL Publ. 97-4, Jet Propulsion Laboratory, Pasadena, CA.

Derwent, R. G.: 1990, *Trace Gases and their Relative Contribution to the Greenhouse Effect*, AERE Report R-13716, H.M. Stationery Office, London.

Edwards, J. M. and Slingo, A.: 1996, 'Studies with a Flexible New Radiation Code. I: Choosing a Configuration for a Large-Scale Model', *Quart. J. Roy. Meteorol. Soc.* **122**, 689–719.

Ehhalt, D. H.: 1974, 'The Atmospheric Cycle of Methane', *Tellus* **26**, 58–70.

Fuglestvedt, J. S., Berntsen, T., Isaksen, I. S. A., Mao, H., Liang, X. Z., and Wang, W. C.: 1999, 'Climatic Forcing of Nitrogen Oxides through Changes in Tropospheric Ozone and Methane; Global 3-D Model Studies', *Atmos. Environ.* **33**, 961–977.

IPCC: 1990, *Climate Change: The IPCC Scientific Assessment*, Cambridge University Press, Cambridge.

IPCC: 1995, *Radiative Forcing of Climate Change. The 1994 Report of the Scientific Assessment Working Group of the IPCC*, WMO UNEP, Geneva, Switzerland.

IPCC: 1996, *Climate Change 1995: The IPCC Scientific Assessment*, Cambridge University Press, Cambridge.

IPCC: 1999, *Aviation and the Global Atmosphere*, Cambridge University Press, Cambridge.

Isaksen, I. S. A. and Hov, O.: 1987, 'Calculation of Trends in the Tropospheric Concentration of $O_3$, OH, CO, $CH_4$ and $NO_x$', *Tellus* **B33**, 271–285.

Johnson, C. E. and Derwent, R. G.: 1996, 'Relative Radiative Forcing Consequences of Global Emissions of Hydrocarbons, Carbon Monoxide and $NO_x$ from Human Activities Estimated with a Zonally-Averaged Two-Dimensional Model', *Clim. Change* **34**, 439–462.

Kanikadou, M., Dentener, F. J., Brasseur, G. P., Berntsen, T. K., Collins, W. J., Hauglustaine, D. A., Houweling, S., Isaksen, I. S. A., Krol, M., Lawrence, M. G., Muller, J. F., Poisson, N., Roelofs, G. J., Wang, Y., and Wauben, W. M. F.: 1999, '3-D Global Simulations of Tropospheric CO

Distributions – Results of the GIM/IGAC Intercomparison 1997 Exercise', *Chemosphere: Global Change Sci.* **1**, 263–282.

Kanakidou, M., Dentener, F. J., Brasseur, G. P., Collins, W. J., Berntsen, T. K., Hauglustaine, D. A., Houweling, S., Isaksen, I. S. A., Krol, M., Law, K. S., Lawrence, M. G., Muller, J. F., Plantevin, P. H., Poisson, N., Roelofs, G. J., Wang, Y., and Wauben, W. M. F.: 1998, *3-D Global Simulations of Tropospheric Chemistry with Focus on Ozone Distributions*, EUR 18842 Report, European Commission, Office for Official Publications of the European Communities, Luxembourg.

Lacis, A. A., Wuebbles, D. J., and Logan, J. A.: 1990, 'Radiative Forcing of Climate by Changes in the Vertical Distribution of Ozone', *J. Geophys. Res.* **95**, 9971–9981.

Leighton, P. A.: 1961, *Photochemistry of Air Pollution*, Academic Press, New York.

Levy, H.: 1971, 'Normal Atmosphere: Large Radical and Formaldehyde Concentrations Predicted', *Science* **173**, 141–143.

Murphy, D. M. and Fahey, D. W.: 1994, 'An Estimate of the Flux of Stratospheric Reactive Nitrogen and Ozone into the Troposphere', *J. Geophys. Res.* **99**, 5325–5332.

Olivier, J. G. J., Bouwman, A. F., van der Maas, C. W. M., Berdowski, J. J. M., Veldt, C., Bloos, J. P. J., Visschedijk, A. J. H., Zandveld, P. Y. J., and Haverlag, J. L.: 1996, *Description of EDGAR Version 2.0*, RIVM Report nr. 771060 002, Bilthoven, The Netherlands.

Olson, J., Prather, M., Berntsen, T., Carmichael, G., Chatfield, R., Connell, P., Derwent, R., Horowitz, L., Jin, S., Kanakidou, M., Kasibhatla, P., Kotamarthi, R., Kuhn, M., Law, K., Penner, J., Perliski, L., Sillman, S., Stordal, F., Thompson, A., and Wild, O.: 1997, 'Results from the Intergovernental Panel on Climatic Change Photochemical Model Intercomparison (Photocomp)', *J. Geophys. Res.* **102**, 5979–5991.

Penner, J. E., Atherton, C. S., Dignon, J., Ghan, S. J., Walton, J. J., and Hameed, S.: 1991, 'Tropospheric Nitrogen: A Threedimensional Study of Sources, Distributions and Deposition', *J. Geophys. Res.* **96**, 959–990.

Penner, J. E., Atherton, C. S., and Graedel, T. E.: 1994, 'Global Emissions and Models of Photochemically-Active Compounds', in Prinn, R. G. (ed.), *Global Atmospheric Biospheric Chemistry*, Plenum Press, New York, pp. 223–247.

Prather, M. J.: 1994, 'Lifetimes and Eigenstates in Atmospheric Chemistry', *Geophys. Res. Lett.* **21**, 801–804.

Prinn, R. G., Weiss, R. F., Miller, B. R., Huang, J., Alyea, F. N., Cunnold, D. M., Fraser, P. J., Hartley, D. E., and Simmonds, P. G.: 1995, 'Atmospheric Trends and Lifetime of $CH_3CCl_3$ and Global OH Concentrations', *Science* **269**, 187–192.

Ramanathan, V., Callis, L., Cess, R., Hansen, J., Isaksen, I., Kuhn, W., Lacis, A., Luther, F., Mahlman, J., Reck, R., and Schlesinger, M.: 1987, 'Climate-Chemical Interactions and Effects of Changing Atmospheric Trace Gases', *Rev. Geophys.* **25**, 1441–1482.

Simmonds, P. G., Derwent, R. G., O'Doherty, S., Ryall, D. B., Steele, L. P., Langenfelds, R. L., Salameh, P., Wang, H. J., Dimmer, C. H., and Hudson L. E.: 2000, 'Continuous High-Frequency Observations of Hydrogen at the Mace Head Baseline Atmospheric Monitoring Station over the 1994–1998 Period', *J. Geophys. Res.* **105**, 12105–12121.

Stevenson, D. S., Collins, W. J., Johnson, C. E., and Derwent, R. G.: 1998, 'Intercomparison and Evaluation of Atmospheric Transport in a Lagrangian Model (STOCHEM), and an Eulerian model (UM), Using $^{222}$Rn as a Short-Lived Tracer', *Quart. J. Roy. Meteorol. Soc.* **124**, 2477–2491.

Stevenson, D. S., Johnson, C. E., Collins, W. J., Derwent, R. G., and Shine, K. P.: 1998, 'Evolution of Tropospheric Ozone Radiative Forcing', *Geophys. Res. Lett.* **25**, 3819–3822.

Walton, J., MacCracken, M., and Ghan, S.: 1988, 'A Globalscale Lagrangian Trace Species Model of Transport, Transformation, and Removal Processes', *J. Geophys. Res.* **93**, 8339–8354.

WMO: 1999, *Scientific Assessment of Ozone Depletion: 1988*, Global Ozone Research and Monitoring Project – Report No. 44, World Meteorological Organization, Geneva, Switzerland.

(Received 1 February 2000; accepted 5 October 2000)